The Journal of Experimental Biology 209, 2025-2033
Published by The Company of Biologists 2006
doi:10.1242/jeb.02242

Fast-swimming hydromedusae exploit velar kinematics to form an optimal vortex wake

John O. Dabiri[1,*], Sean P. Colin[2] and John H. Costello[3]

[1]*Graduate Aeronautical Laboratories and Bioengineering, California Institute of Technology, Mail Code 138-78, Pasadena, CA 91125, USA,* [2]*Biology and Marine Biology, Roger Williams University, MNS 241, Bristol, RI 02809, USA and* [3]*Biology, Providence College, Providence, RI 02918, USA*

*Author for correspondence (e-mail: jodabiri@caltech.edu)

Accepted 27 March 2006

Summary

Fast-swimming hydromedusan jellyfish possess a characteristic funnel-shaped velum at the exit of their oral cavity that interacts with the pulsed jets of water ejected during swimming motions. It has been previously assumed that the velum primarily serves to augment swimming thrust by constricting the ejected flow in order to produce higher jet velocities. This paper presents high-speed video and dye-flow visualizations of free-swimming *Nemopsis bachei* hydromedusae, which instead indicate that the time-dependent velar kinematics observed during the swimming cycle primarily serve to optimize vortices formed by the ejected water rather than to affect the speed of the ejected flow. Optimal vortex formation is favorable in fast-swimming jellyfish because, unlike the jet funnelling mechanism, it allows for the minimization of energy costs while maximizing thrust forces. However, the vortex 'formation number' corresponding to optimality in *N. bachei* is substantially greater than the value of 4 found in previous engineering studies of pulsed jets from rigid tubes. The increased optimal vortex formation number is attributable to the transient velar kinematics exhibited by the animals. A recently developed model for instantaneous forces generated during swimming motions is implemented to demonstrate that transient velar kinematics are required in order to achieve the measured swimming trajectories. The presence of velar structures in fast-swimming jellyfish and the occurrence of similar jet-regulating mechanisms in other jet-propelled swimmers (e.g. the funnel of squid) appear to be a primary factor contributing to success of fast-swimming jetters, despite their primitive body plans.

Supplementary material available online at
http://jeb.biologists.org/cgi/content/full/209/11/2025/DC1

Key words: locomotion, wake, vortices, jellyfish, *Nemopsis bachei*.

Introduction

Pulsatile jet propulsion is one of the earliest known forms of aquatic locomotion exhibited by animals. Using a simple action–reaction principle, jet-propelled animals move forward by periodically ejecting jets of water in a direction opposite to the desired trajectory. Hydromedusan jellyfish have been especially successful in implementing this strategy. For example, measurements of *Aglantha digitale* medusae suggest that swimming speeds above 13 body lengths (*BL*) s^{-1} are achieved during fast-swims, outpacing all but the very fastest predatory bony fishes [albeit for short bursts (Mackie, 1980; Donaldson et al., 1980)]. In cnidarians such as *Aglantha*, the jetting strategy is the sole means of propulsion. By contrast, some higher organisms such as cephalopods make use of pulsed jets primarily for high-speed swimming (e.g. squid in their tail-first configuration), relying on lateral fins for locomotion at low speeds (Bartol et al., 2001; Anderson and Grosenbaugh, 2005).

The body plan of hydromedusan jellyfish is most commonly prolate, or torpedo-shaped, consistent with the need to reduce resistive forces associated with their rapid swimming accelerations. This acceleration reaction, the effect of body added-mass (Daniel, 1983), is reduced for more prolate body shapes. In addition, these animals possess a characteristic funnel-shaped velum at the exit of their oral cavity. In a resting position, the velum is oriented in a plane perpendicular to the body axis of radial symmetry (Fig. 1A). As water is ejected from the subumbrellar oral cavity, the generated fluid pressure causes the velum to 'outpocket', effectively creating a funnel through which the jet flow emerges (Fig. 1B). The velum has therefore been assumed to function primarily as a flow accelerator, augmenting thrust *via* an increase in jet flow velocity through the funnel. However, improved thrust generation by this mechanism would be achieved at the expense of increased costs of locomotion (Gladfelter, 1972; Daniel, 1983; Daniel, 1985).

The flow created by pulsatile jets is dominated by radially symmetric, rotating currents called vortex rings. Laboratory studies using mechanical pulsatile jet generators have shown that a physical limit exists on the maximum size of any vortex ring created by a pulsatile jet. Once this limit – called the vortex 'formation number' (denoted T^*_{lim}, where the asterisk indicates that the parameter is dimensionless) – is reached, additional fluid ejected during the same pulse forms a jet of fluid that trails behind the vortex ring (Gharib et al., 1998). The energy cost of ejecting fluid in the form of a vortex ring with a trailing jet behind it has been shown to be higher than fluid transport *via* an isolated vortex ring with no trailing jet (Krueger and Gharib, 2003). Together, these results suggest that the efficiency of fluid transport in pulsatile jets can be maximized by the formation of 'optimal' vortex rings, in the sense of the largest possible vortex during each jet pulse without the formation of a trailing jet behind the vortex.

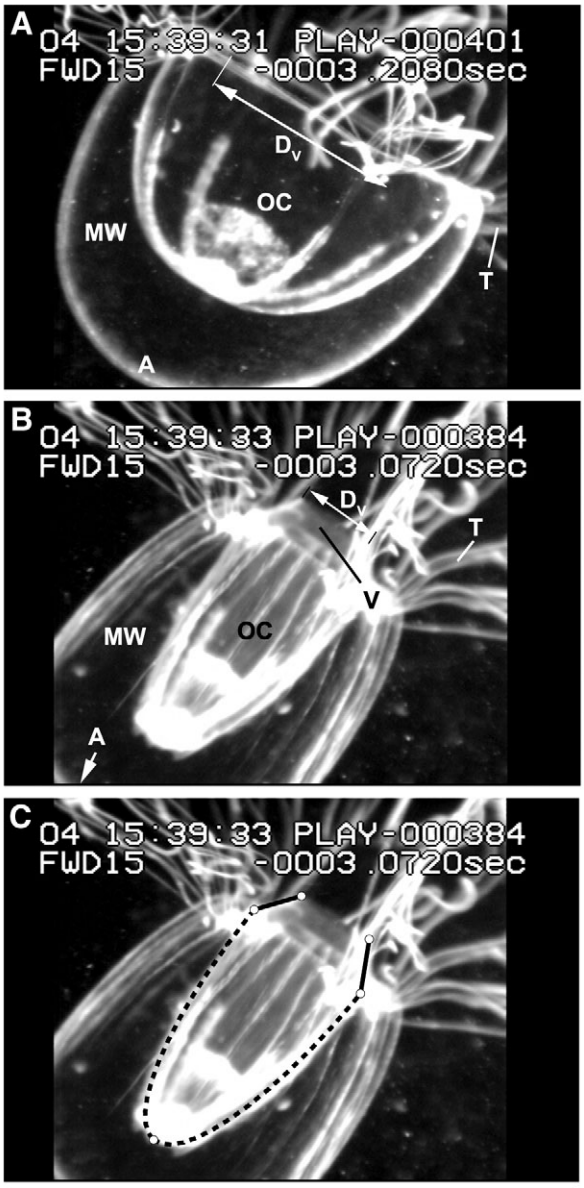

Fig. 1. Morphological analysis of *N. bachei*. (A,B) Images of *N. bachei* (A) at rest, and (B) during jet ejection. Image height is 7.2 mm. V, velum; D_V, velar diameter; T, tentacles; OC, oral cavity; MW, mesogleal wall; A, animal apex. Out-pocketing of velum into funnel shape is discernable in B. (C) Sample of image analysis. Image from B superimposed with reconstructions of the oral cavity boundary (broken black line) and velum (solid black line), based on control points (white circles).

Given the broad role of pulsatile jet propulsion in a diverse range of biological fluid transport functions, from aquatic locomotion to intracardiac blood transport, it is useful to ask whether animal systems are capable of optimizing vortex formation to take advantage of the aforementioned functional benefits discovered in mechanical fluid transport systems. A key difference between the mechanically generated jet flows previously studied and those occurring in nature is the appearance of valve-like structures, such as the hydromedusan velum described above, which vary the jet exit diameter during the vortex formation process. It has recently been shown that a proper extension of the optimal vortex formation concept to animal systems must incorporate these time-dependent kinematics in the analysis (Dabiri and Gharib, 2005a; Dabiri and Gharib, 2005b). Failure to do so can obscure the importance of optimal vortex formation to biological fluid transport processes. In particular, time-dependent valve (or similar structure) kinematics are capable of changing the optimal vortex formation number T^*_{lim} from the specific value $T^*_{lim} \approx 4(\pm 0.5)$ found in constant-diameter mechanically generated jets (Dabiri and Gharib, 2005b). Consequently, the existence of optimal vortex formation (or a lack thereof) in a biological system cannot be proven based on the assumption of a particular numerical value of the vortex formation number.

To better understand the role of optimal vortex formation in biological pulsed jets, this paper investigates the possible occurrence of optimal vortex formation in the fast-swimming jellyfish *Nemopsis bachei* Agassiz 1849. First, we use high-speed video imaging of free-swimming specimens to measure the time-dependent velar kinematics during the entire swimming cycle. Second, we combine these results with dye flow visualization of the wake created by *N. bachei* and a model for the associated swimming dynamics to determine whether the animal achieves optimal vortex formation, in a manner similar to that observed in recent mechanically generated jet flow experiments (Dabiri and Gharib, 2005b). In the process, generally applicable aspects of the optimal vortex formation concept are identified.

Materials and methods

Video measurements and analysis

Specimens of *Nemopsis bachei* Agassiz (*BL* ~5 mm) were placed in a Petri dish filled with saltwater and observed under a light microscope. Swimming motions were elicited using tactile stimulation from an external needle brought in contact

with the tentacles. The results were recorded digitally from a 720×480 pixel CCD camera to a PC at 250 frames s^{-1}. Motion of the velum was observed from camera views into the oral cavity (from an oblique angle) and from the side during separate swimming cycles, to ensure that the velum was properly identified. In addition, a larger-field view was used during separate swimming cycles to observe the wake created by the animals. This wake flow was made visible by injecting a milk solution into the oral cavity prior to the introduction of the tactile stimulation that elicited swimming motions. Since not all of the injected dye was ejected during each contraction phase, residual dye in the subumbrellar region facilitated visualizations of the subsequent refilling phase as well.

Image analysis (Dabiri and Gharib, 2003) was used to reconstruct the animal morphology and kinematics based on the manually selected locations of the apex of the subumbrellar oral cavity, the edges of the subumbrellar margin, and the velar tips, as observed in each frame of the video measurements (Fig. 1C). The algorithm then created a best-fit curve connecting the selected control points. The fidelity of each morphological reconstruction was confirmed based on comparison with local image intensity and contrast signatures in the original image frame. Given the approximation that the animals are radially symmetrical [reasonable for the present analysis (Gladfelter, 1972)], the elliptical reconstruction (e.g. Fig. 1C) was sufficient to compute the volume of the oral cavity for each video frame captured during the swimming cycles. Volume measurements possess a maximum uncertainty of ±6%, stemming from determination of the oral cavity boundary (i.e. broken curve in Fig. 1C).

Due to inherent challenges in capturing the rapid swimming motions in a manner such that they could be subsequently analyzed quantitatively (e.g. motion in a plane parallel to the camera image plane and away from the Petri dish bottom, straight swimming trajectories that are contained in the field of view, etc.), the number of specimens that could be examined quantitatively was limited (N=2). These animals exhibited behavior that was qualitatively and quantitatively similar when investigated in depth. However, the generality of the quantitative conclusions that can be drawn from this study is necessarily tempered by the limited sample size. In the subsequent presentation of measurements, two distinct swimming cycles are presented as an indication of the repeatability of the phenomena observed here.

Vortex formation parameter

The vortex 'formation time', the dimensionless parameter which is used to describe the vortex formation process, can be generalized (Dabiri and Gharib, 2005a; Dabiri and Gharib, 2005b) to the case of a time-varying jet velocity $U(t)$ and diameter $D(t)$ by expressing the parameter as an integral:

$$T^* = \int_0^t \frac{U(\tau)}{D(\tau)}\, d\tau\,, \tag{1}$$

where time t=0 corresponds to the start of fluid ejection (e.g. the beginning of medusa bell contraction). A complementary modification (Krueger et al., 2004) can be incorporated in Eqn 1 to account for flow past the animal (irrespective of the animal shape) that occurs due to forward motion of the animal relative to the surrounding fluid:

$$T^* = \int_0^t \frac{U(\tau) + \dot{X}(\tau)}{D(\tau)}\, d\tau\,, \tag{2}$$

where $\dot{X}(t)$ is the instantaneous forward velocity of the animal. The vortex formation time parameter in Eqn 2 was computed for the *N. bachei* specimens based on the measured forward velocity $\dot{X}(t)$ as well as the measured oral cavity volume $V_{OC}(t)$ and velar diameter $D_V(t)$:

$$T^* = \int_0^t \frac{\dfrac{-4dV_{OC}(\tau)/d\tau}{\pi D_V^2(\tau)} + \dot{X}(\tau)}{D_V(\tau)}\, d\tau\,. \tag{3}$$

Note that the first term in the numerator of Eqn 3 is the jet velocity during fluid ejection and is positive since the oral cavity volume is decreasing during fluid ejection.

Fluid dynamic model

The measured body kinematics, $V_{OC}(t)$ and $D_V(t)$, of swimming *N. bachei* were input to a recently developed force estimation model (Dabiri, 2005) to discern the effect of velar kinematics on the swimming performance predicted by the model. In the model (Dabiri, 2005), the magnitude of the swimming force $\mathbf{F}_L$ generated by *N. bachei* during the contraction phase is dictated by the transfer of momentum from the animal to the wake in the form of fluid vorticity (rotation and shear) and wake vortex added-mass (cf. Dabiri, 2006), an unsteady contribution from the acceleration of the fluid vorticity.

It is important to note that the governing equation for force estimation in Dabiri's model (Dabiri, 2005) contains an error that is corrected here [see Appendix and published Corrigendum (Dabiri, 2005)]. The correct equation for the locomotive force, in its most general form, is:

$$\mathbf{F}_L = \rho \frac{d}{dt}\left[(\mathbf{1}+\mathbf{C}_{\mathbf{AM}}^{-1}) \int_{S_V} \phi \mathbf{n} dS\right], \tag{4}$$

where ρ is the density of the fluid (water), $\mathbf{1}$ is the identity matrix (a matrix with each diagonal element equal to 1), $\mathbf{C}_{\mathbf{AM}}$ is the wake vortex added-mass tensor (a 3×3 matrix in the present case), ϕ is the velocity potential, and the normal vector $\mathbf{n}$ is directed out of the vortex wake. The integral is evaluated on the surface S_V of the vortex wake. The added-mass tensor of a vortex will typically have non-zero elements only on the diagonal (see Appendix). Hence, the matrix inverse $\mathbf{C}_{\mathbf{AM}}^{-1}$ in Eqn 4 can be evaluated in an element-wise fashion.

The integral of the velocity potential in Eqn 4 can be expressed in terms of the volume $V_V(t)$ and velocity $\mathbf{U_V}(t)$ of the vortex wake (see Appendix):

$$\mathbf{F}_L(t) = -\rho \frac{d}{dt}\left[(\mathbf{1}+\mathbf{C}_{AM})\mathbf{U_V}(t)V_V(t)\right] . \quad (5)$$

The volume $V_V(t)$ of the wake vortex created by *N. bachei* during each swimming cycle was calculated by assuming that all of the fluid ejected during a pulse is contained in the generated wake vortex, and that an additional volume of fluid equal to 30% of the vortex volume was also entrained into the wake vortex from the ambient fluid:

$$V_V(t) = \left[\frac{1}{(1–0.3)}\right]\left(\frac{\pi}{4}\right)\int_0^t U(\tau)D^2(\tau)d\tau , \quad (6)$$

or, using the present measurement data,

$$V_V(t) = \left[\frac{1}{(1–0.3)}\right]\int_0^t\left[\frac{-dV_{OC}(\tau)}{d\tau}\right]d\tau . \quad (7)$$

The assigned 30% entrainment is compatible with laboratory studies of vortex formation from pulsed jets (Dabiri and Gharib, 2004).

The vortex velocity $\mathbf{U_V}(t)$ was approximated as the ratio of the vortex ring circulation $\Gamma(t)$ to the vortex ring radius $R(t)$. The circulation was estimated using the 'slug model' (Didden, 1979), which assumes that fluid is initially ejected as a straight, spatially uniform jet. With this assumption, the model gives:

$$\Gamma(t) = \frac{1}{2}\int_0^t U^2(\tau)d\tau , \quad (8)$$

or, using the present measurement data,

$$\Gamma(t) = \frac{1}{2}\int_0^t\left\{\left[\frac{-4dV_{OC}(\tau)/d\tau}{\pi D_V^2(\tau)}\right]^2 - [\dot{X}(\tau)]^2\right\}d\tau . \quad (9)$$

The second term in Eqn 9 reflects the fact that flow past the animal reduces the relative strength (i.e. circulation content) of the ejected jet by reducing its velocity relative to the ambient flow (Krueger et al., 2003; Krueger et al., 2006). The vortex radius $R(t)$ was derived from the volume calculation in Eqn 7 as:

$$R(t) \approx \left[\frac{3}{4\pi}V_V(t)\right]^{1/3} . \quad (10)$$

Finally, dye visualizations (e.g. Fig. 4) indicated that that the wake vortex ring created by *N. bachei* is closely approximated by an ellipsoid with added-mass coefficient c_{ii}=0.6 in the axial direction. This component of the full added-mass tensor is the only one of relevance since the net locomotive force is aligned with the axial direction. Combining Eqn 5, Eqn 7, Eqn 9 and Eqn 10, the complete equation for the locomotive force $\mathbf{F}_L$ deduced from the measurements of the *N. bachei* wake is:

$$\mathbf{F}_L(t) = -A\rho\frac{d}{dt}\left(\frac{\displaystyle\int_0^t\left\{\left[\frac{-4dV_{OC}(\tau)/d\tau}{\pi D_V^2(\tau)}\right]^2 - [\dot{X}(\tau)]^2\right\}d\tau}{\displaystyle\left\{\int_0^t\left[\frac{-dV_{OC}(\tau)}{d\tau}\right]d\tau\right\}^{1/3}}\int_0^t\frac{-dV_{OC}(\tau)}{d\tau}d\tau\right)\mathbf{e_1} , \quad (11)$$

where $\mathbf{e_1}$ is a unit vector in the axial swimming direction and the parameter A is a constant equal to 1.63 in the present case. In general, A will depend on the shape of the wake vortex (*via* dependence on the added-mass coefficient, vortex entrainment, and the assumed relationship between vortex radius and volume in Eqn 10), but the functional form of Eqn 11 will remain the same. Hence, we are able to estimate the force produced by a jet-propelled animal based solely on the body kinematics $V_{OC}(t)$ and $D_V(t)$. Since Eqn 11 also requires knowledge of the instantaneous forward swimming velocity $\dot{X}(t)$, the equations must be solved iteratively. To do so, the animal was assumed to begin its motion from rest [$\dot{X}(0)$=0] and the swimming velocity was modelled based on the instantaneous swimming acceleration $\ddot{X}(t)$ derived from Newton's law:

$$\dot{X}(t) = \int_0^t\ddot{X}(\tau)d\tau = \int_0^t\frac{\|\mathbf{F}_L(\tau)\|}{m}d\tau , \quad (12)$$

where m is the mass of the animal, estimated from the body volume and by assuming that the animal is neutrally buoyant (i.e. $\rho_{body}=\rho_{fluid}$). The swimming trajectory $X(t)$ was computed by integrating the forward swimming velocity in Eqn 12 over the duration of the swimming cycle.

To complete the model of swimming dynamics, the refilling phase was assumed to consist of a spatially uniform inflow (Daniel, 1983). This assumption is consistent with dye visualizations of the refilling phase (see Results), which did not indicate the prominent vortex formation that has been seen in a recent study of the oblate schyphozoan refilling phase (Dabiri et al., 2005).

It is important to note that the swimming model (Eqn 12) does not include the effects of any resistive fluid dynamic forces. This omission stems from the fact that the required measurements of the oral cavity and velar kinematics could not be obtained from a view that contained the full exumbrellar surface. This outer surface profile is necessary in order to estimate both viscous drag and the acceleration reaction (added-mass) of the animal body. Although this deficiency limits comparison between the measurements and models to a qualitative analysis, it will be shown that qualitative comparison alone is sufficient to demonstrate the importance of velar kinematics for the observed swimming performance.

Results

Fig. 2 shows that the velar diameter changes in phase with the subumbrellar cavity volume, indicating that contraction of the velum during bell contraction dictates velar kinematics to a greater degree than the out-of-phase outpocketing effect as the velum swings open. At the end of jet ejection, the velum has decreased to one-fifth of its resting diameter, or 4% of its resting area. The superimposed data from a single swimming contraction of each animal (Fig. 2) suggests the level of inter-animal repeatability of the observed velar kinematics.

Calculation of the vortex formation time of the ejected jet based on the measured *N. bachei* kinematics (i.e. Eqn 3) evaluated over the duration of the contraction phase) indicates that swimming function of the *N. bachei* sample achieves a total vortex formation time $T^*_{max}\approx 8$, greater than the vortex formation number that was observed in studies of rigid tube pulsed jets to coincide with the limit of vortex growth, $T^*_{lim}\approx 4$ (Fig. 3). If vortex growth had ceased at any value of T^* prior to end of the ejection phase [i.e. any $T^*_{lim}<T^*_{max}$), a pronounced trailing jet of fluid would be observed directly behind the vortex [e.g. see fig. 3C (Gharib et al., 1998)].

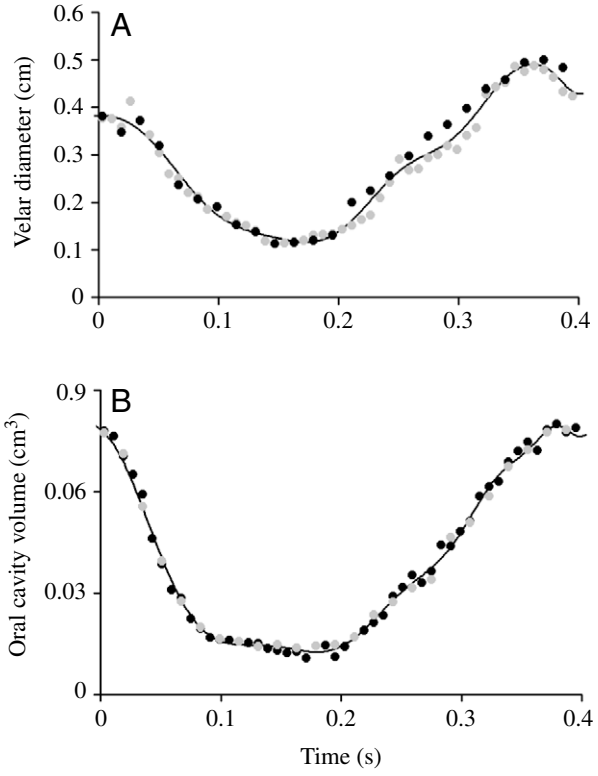

Fig. 2. Measurements of *N. bachei* body kinematics during fast swimming. Two sets of measurements from distinct swimming cycles from two different animals (black and grey circles) are presented to indicate the repeatability of the swimming motions. Maximum measurement uncertainty is ±6%. A curve fit to the data (solid black line) is used in subsequent analyses. (A) Velar diameter *versus* time during the swimming cycle. (B) Oral cavity volume *versus* time during the swimming cycle.

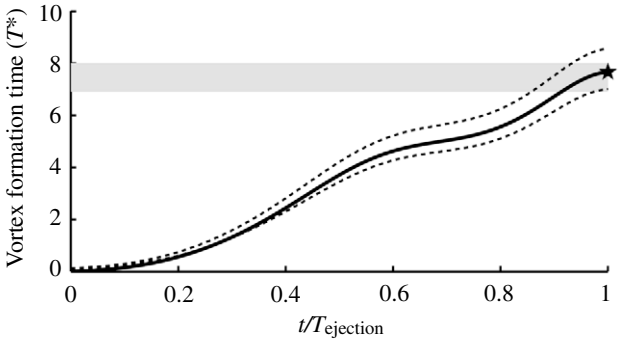

Fig. 3. Plot of vortex formation time (T^*) during the jet ejection phase ($t/T_{ejection}$) of the swimming cycle (solid black line). At the end of the ejection phase (black star), the vortex formation time coincides with the range of values producing maximum vortex growth in mechanically generated jet flows with similar aperture kinematics (grey band) (Dabiri and Gharib, 2005b), where the aperture diameter contraction rate ranges between 15% and 30% of the average jet velocity. For comparison, the measured velar aperture contraction rate in *N. bachei* is approximately 20% of the average jet velocity. Broken lines indicate measurement uncertainty of ±10% associated with calculation of vortex formation time (see Materials and methods). Note that the local plateau in the vortex formation time near $t/T_{ejection}$=0.7 is within the error of the measurement trend.

However, visualization of the wake of the *N. bachei* (Fig. 4) conclusively demonstrates that the animals do in fact create only a single vortex without a trailing jet during each jet ejection phase, despite the fact that the total vortex formation time T^*_{max} is much greater than 4. This result is examined further in the Discussion.

The importance of temporal variations in the velar diameter becomes apparent when one examines their effect on the forward trajectory of the animal. Fig. 5 plots the measured trajectory of a *N. bachei* specimen during a single swimming

Fig. 4. Optimal vortex formation during fast-swimming of *N. bachei*. Image from dye flow visualization showing vortex formation in the wake of the animal. Image height is 7.2 mm. No trailing flow exists directly behind the vortex (see also movie in supplementary material), supporting the conclusion that the animal generates a single vortex (shown schematically in inset) per swimming cycle, despite the fact that $T^*_{max}\approx 8$.

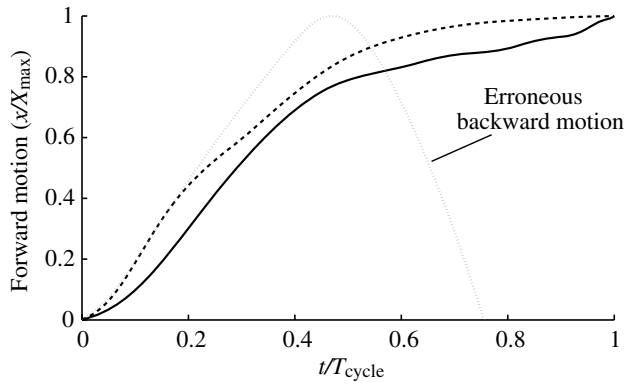

Fig. 5. Measurement and models of *N. bachei* swimming trajectory. The ratio of instantaneous forward motion (relative to its position at the start of the measured swimming cycle) to the maximum forward motion, x/X_{max}, is plotted *versus* the current point in the full swimming cycle (i.e. ejection and relaxation). Both the real animal (solid black line) and the model that includes transient velar kinematics (broken black line) achieve continuous forward motion, whereas the model that assumes a constant velar aperture (dotted grey line) swims backward during the latter portion of the swimming cycle. Measurement uncertainty is ±3%.

cycle (solid black line) and compares this with the aforementioned model (Dabiri, 2005) of the trajectory (Eqn 11, Eqn 12) based on either the measured time-varying velar kinematics (broken black line) or a hypothetical constant velar diameter (equal to the velar diameter at rest; dotted grey line). The results in Fig. 5 are presented such that the measured trajectory and the models each have the same maximum forward motion. This presentation provides an objective comparison despite the fact that the effect of resistive fluid forces is not included in the models, as mentioned previously. The swimming model based on transient velar kinematics agrees qualitatively with the trend observed empirically, while the model assuming a constant velar diameter does not. Specifically, a constant velar aperture would result in a significant backward motion of the animal during the refilling phase. In contrast, thrust generated during the ejection phase of the animals (real and modelled) with time-varying velar kinematics is sufficient to fully compensate for the retarding effect of the refilling phase. Hence, this qualitative comparison suggests that the velar motion exhibited by *N. bachei* is integral to the observed swimming performance of the animals.

An important component of the dynamic model for the refilling phase was the assumption that vortex ring formation does not affect this portion of the swimming cycle in hydromedusae, and therefore the refilling flow may be treated as a uniform inflow jet (Daniel, 1983). Dye visualizations support this assumption from two perspectives. First, the vortex ring formed during the contraction phase has moved sufficiently far downstream at the end of the contraction phase that the flow field it induces at the subumbrellar margin is negligible (Fig. 4). The magnitude of the flow induced by the vortex is inversely proportional to the distance from the vortex (Lamb, 1932). Second, there is no visual evidence of a pronounced stopping vortex during the refilling phase (see movie in supplementary material), as has been observed in scyphomedusae (Dabiri et al., 2005).

Discussion

Small hydromedusae swim in order to escape predation and to reposition themselves to feed (Colin et al., 2003). Effective swimming for these small hydromedusae means that they are capable of accelerating fast enough to avoid predation and efficiently enough to avoid wasting valuable energy resources. We have demonstrated that *N. bachei* is able to manipulate its velar diameter during swimming in a manner that enables the medusa to produce a jet that maximizes thrust while minimizing energy costs. Specifically, contracting the velum during bell contraction resulted in *N. bachei* being able to achieve a total formation time $T^*_{max}\approx 8$ while producing only a single vortex (i.e. without a thick trailing jet directly behind it).

Previous analyses (e.g. Gharib et al., 1998) have demonstrated that it is not possible to form a single vortex from a jet ejected with a total vortex formation time $T^*_{max}\approx 8$ if the velar diameter is constant (given that the corresponding vortex formation number T^*_{lim} for a pulsed jet ejected from a constant-diameter orifice or nozzle is equal to 4). Based on studies with constant aperture area jets, total vortex formation times $T^*_{max}>4$ indicate that jet ejection continued beyond the formation number (i.e. the formation time at which vortex growth ceases) and that they are not functioning in an energetically efficient manner. However, mechanically generated jet flows exhibiting a temporally variable aperture area (Dabiri and Gharib, 2005b) suggest that the rate of velar diameter decrease achieved by *N. bachei* (approximately 20% of the average jet velocity) is sufficient to extend vortex growth beyond $T^*\approx 4$. In the mechanically generated jet flows, aperture diameter contraction rates between 15% and 30% of the average jet velocity were sufficient to prolong vortex growth. Although the velar geometry and kinematics in those experiments were not identical to those of *N. bachei* (e.g. the velar motion was prescribed *a priori*), the vortex formation process in both cases shares similar physics.

It is also observed that at the end of the ejection phase of swimming motions, the vortex formation time exhibited by *N. bachei* ($T^*\approx 8$) coincides very closely with the time at which vortex growth is expected to terminate, based on those previous mechanical experiments (Fig. 3). Together, these results suggest that *N. bachei* creates a single vortex during the contraction phase of each swimming cycle and that the vortex is the largest that can be achieved with its given velar kinematics, since the duration of jet ejection coincides with the duration of vortex growth. Hence, optimal vortex formation is achieved *via* the velar motions, in the sense of the largest possible vortex without the formation of a trailing jet directly behind the vortex. This results in a maximization of swimming thrust while avoiding the penalty of increased

energetic costs that is associated with the formation of a trailing jet.

Our results demonstrate that the velum functions to tune fluid ejection, achieving efficient swimming by exploiting the concept of optimal vortex formation. Important differences may potentially exist between the manifestation of optimal vortex formation in simplified laboratory experiments and the real animals, especially in the value of the vortex formation number parameter. These differences must be appreciated in comparative biological analyses, lest spurious conclusions be reached regarding the structure–function relationships exhibited by these animals. The time-dependent velar motion has been shown to be integral to the observed swimming performance. The model prediction of backward swimming motion for a constant velar diameter is consistent with previous observations of reduced swimming performance in hydromedusae with the velum excised (Gladfelter, 1972).

It is important to note the possibility of even further improved swimming performance in other aquatic jet-propelled swimmers. While in the present case vortex growth was extended until $T^*\approx 8$, recent theoretical studies suggest that vortex formation can, in principle, be extended by another 35%, approaching $T^*\approx 11$ (Kaplanski and Rudi, 2005). This room for improvement may already be occupied by jetters whose performance is known to surpass that of *Nemopsis bachei*, such as *Aglantha digitale* (Colin and Costello, 2002).

The discussion of swimming energetics has thus far focused on the vortex wake created by *N. bachei*. It is useful to consider also whether the shape of the subumbrellar region and the velum may inherently pose energetic benefits for locomotion outside of the aforementioned wake dynamics. Engineering studies of flow exiting through orifices and nozzles have demonstrated that fluid energy losses are a direct function of the exit boundary shape (Smits, 2000). As a rigid structure, the resting orientation of the *N. bachei* velum in a plane normal to the jet flow would promote flow separation upstream of the velar exit, resulting in energy losses during the process of fluid ejection. By contrast, the outpocketed nozzle configuration of the velum during the contraction phase minimizes upstream flow separation. We therefore hypothesize that the flow-induced deformation of the velum from its resting configuration to the outpocketed nozzle shape is a passive mechanism that functions to minimize shape-related energy losses during the swimming cycle. Although the same benefit to the contraction phase could be achieved by a rigid velum in the outpocketed configuration, the flow during the refilling phase would be made much less efficient. The resting position of the velum and its flexibility together enable flow-induced forces to create an energy-preserving nozzle passage during both fluid ejection and refilling, whereas a rigid outpocketed velum could not. The energy required to deform the elastic velum in the process is likely negligible.

Finally, the concept of optimal vortex formation is not limited to the formation of single vortices. Some species of jetting squid are known to form a thick trailing jet flow directly behind the vortex, indicating that jet ejection is continued after vortex growth has ceased (Anderson and Grosenbaugh, 2005). However, temporal variations in the aperture area can still be coordinated with the vortex formation time T^* for alternative behavioural aims, such as the maximization of absolute thrust magnitude, irrespective of the required energy input (Dabiri and Gharib, 2005a). Such a behaviour would be appropriate in life-threatening circumstances, such as during escape from predators. In each case, the velum or analogous structure appears to be a primary factor contributing to success of fast-swimming jetters, despite their primitive body plans. The appearance of optimal vortex formation as a successful strategy in response to selective pressures at the relatively low Reynolds numbers observed here ($Re<200$) supports that the notion that optimal vortex formation may exist even more broadly in aquatic locomotion and biological propulsion. This suggestion of a broader role for the concept of optimal vortex formation in swimming and flying has been buoyed by recent comparative biomechanics studies at higher Reynolds numbers (Linden and Turner, 2004; Dabiri and Gharib, 2005a; Milano and Gharib, 2005).

Appendix

Derivation of Eqn 4 and revised wake vortex ratio (Wa)

The model of Dabiri aims to include the effect of flow unsteadiness in estimates of locomotive forces based on wake measurements (Dabiri, 2005). Traditional analyses make use of the vortex impulse $\mathbf{I_V}$, which can be computed given the distribution of vorticity in the (assumed three-dimensional) wake:

$$\mathbf{I_V} = \frac{\rho}{2}\int_{V_V} \mathbf{x}\times\boldsymbol{\omega} dV\,. \tag{A1}$$

The vortex impulse accounts for the total linear momentum carried by a vortex if and only if that vortex is moving at its self-induced velocity $\mathbf{U_{SI}}$ (i.e. the velocity induced by the distribution of vorticity on itself). This can be seen more explicitly by rewriting the integral in Eqn A1 using the theorem of Burgatti (Saffman, 1992):

$$\frac{1}{2}\int_{V_V} \mathbf{x}\times\boldsymbol{\omega} dV = \int_{V_V} \mathbf{u} dV - \int_{S_V} \phi\mathbf{n} dS\,. \tag{A2}$$

The first integral on the right-hand side of Eqn A2 is by definition equal to the linear momentum of the fluid inside the wake vortex volume V_V. If the center of mass of the wake vortex moves at $\mathbf{U_{SI}}$ (e.g. the aforementioned case of self-induced motion), we have:

$$\rho\int_{V_V} \mathbf{u} dV = \rho V_V \mathbf{U_{SI}}\,. \tag{A3}$$

The second integral on the right-hand side of Eqn A2 – negative sign included – is the contribution from wake vortex added-mass. By definition, it is equal to the linear momentum

of fluid surrounding the wake vortex volume V_V, and is computed by integrating the velocity potential ϕ on the surface S_V of the wake vortex. The negative sign in Eqn A2 arises from the convention that the unit normal $\mathbf{n}$ is directed out of the wake vortex into the surrounding fluid. This second integral can be expressed in terms of the wake vortex volume V_V and the self-induced vortex velocity $\mathbf{U_{SI}}$ using the wake vortex added-mass tensor $\mathbf{C_{AM}}$:

$$-\rho \int_{S_V} \phi \mathbf{n} dS = \rho V_V \mathbf{C_{AM}} \mathbf{U_{SI}} . \quad \text{(A4)}$$

Substituting Eqn A2–A4 into Eqn A1 and taking the time-derivative, we can deduce that the locomotive force $\mathbf{F}_L$ arising due to the creation of a steady vortex propagating at its self-induced velocity $\mathbf{U_{SI}}$ is given by:

$$\mathbf{F}_L = -\frac{\partial \mathbf{I_V}}{\partial t} = -\frac{\partial}{\partial t}\left(\frac{\rho}{2}\int_{V_V} \mathbf{x} \times \boldsymbol{\omega} dV\right) = -\frac{\partial}{\partial t}\left[\rho V_V (\mathbf{1}+\mathbf{C_{AM}})\mathbf{U_{SI}}\right] , \quad \text{(A5)}$$

where $\mathbf{1}$ is the identity matrix (Lamb, 1932). It is worth re-emphasizing that only in the case of a steady flow can the locomotive force $\mathbf{F}_L$ be deduced solely from the vortex impulse Eqn A1. In general, flow unsteadiness caused by ambient flow conditions (relative to the animal) and any interactions between the wake and the animal body/appendages (e.g. during vortex formation, wake capture, etc.) will cause the vortex wake to propagate at a velocity different from its self-induced velocity $\mathbf{U_{SI}}$. In these cases, the actual vortex motion $\mathbf{U_V}$ replaces the self-induced velocity $\mathbf{U_{SI}}$ in Eqn A3 and Eqn A4. However, their sum,

$$\mathbf{I} = \rho V_V (\mathbf{1}+\mathbf{C_{AM}})\mathbf{U_V} , \quad \text{(A6)}$$

is no longer equivalent to the integral in Eqn A1. Dabiri's equation 4 (Dabiri, 2005) incorrectly accounts for the additional unsteady contribution by adding the added-mass integral in Eqn A4 to the vortex impulse in Eqn A1. The proper solution is to use Eqn A6 in its current form, as done in the present paper. Alternatively, if an integral form is preferred (e.g. for numerical simulations), one can rewrite the identity matrix in Eqn A6 using $\mathbf{1}=\mathbf{C_{AM}}^{-1}\mathbf{C_{AM}}$, factor out the added mass tensor, and use Eqn A4 to arrive at the relation:

$$\mathbf{I} = -\rho(\mathbf{1}+\mathbf{C_{AM}^{-1}}) \int_{S_V} \phi \mathbf{n} dS . \quad \text{(A7)}$$

The locomotive force is then given by Eqn 4. The validity of Eqn A7 is dependent on the wake vortex added-mass tensor being non-singular, so that the matrix inverse can be performed. This does not appear to be a limitation in practice since the presence of fluid viscosity suggests that the wake vortex boundary S_V will typically be geometrically regular (The interested reader is encouraged to pursue a rigorous proof of this statement). When the wake vortex possesses two orthogonal planes of symmetry, the added-mass tensor $\mathbf{C_{AM}}$ will have non-zero elements only along the diagonal. Hence, the inverse can be computed in an element-wise fashion.

Dabiri introduced the wake vortex ratio (Wa) as a measure of the importance of flow unsteadiness to the total locomotive force (Dabiri, 2005). The preceding developments enable us to refine both the definition and quantitative interpretation of the wake vortex ratio. Let us begin with the parameter Wa as defined by Dabiri (Dabiri, 2005):

$$\mathrm{Wa} = \frac{\bar{c}_{ii} S U_{Vi}}{\Gamma} , \quad \text{(A8)}$$

where $\bar{c}_{ii}$ is the two-dimensional approximation for the wake vortex added-mass coefficient corresponding to unidirectional motion in the i-direction, S is the wake vortex width, and U_{Vi} is the total wake vortex speed in the i-direction. The ratio in Eqn A8 compares the linear momentum of the wake vortex added-mass (propagating with the wake vortex at velocity $\mathbf{U_V}$) to the steady vortex momentum (i.e. wake vortex propagation at the self-induced velocity $\mathbf{U_{SI}}$ instead of its actual velocity $\mathbf{U_V}$); for details of the derivation, see (Dabiri, 2005). Eqn A4–A6 indicate that the wake vortex ratio can be written more generally as:

$$\mathrm{Wa} = \frac{\left\|\rho V_V \mathbf{C_{AM}} \mathbf{U_V}\right\|}{\left\|\rho V_V (\mathbf{1}+\mathbf{C_{AM}})(\mathbf{U_V}-\mathbf{U_U})\right\|} , \quad \text{(A9)}$$

where the L_2-norm $\| \|$ denotes the magnitude of the enclosed vector, and $\mathbf{U_U}$ is the unsteady component of the wake vortex velocity, i.e. $\mathbf{U_V}-\mathbf{U_U}=\mathbf{U_{SI}}$. For unidirectional vortex motion in the i-direction, straightforward algebraic manipulation reduces Eqn A9 to:

$$\mathrm{Wa} = \frac{c_{ii}}{1 + c_{ii} - (1+c_{ii})\dfrac{U_{Ui}}{U_{Vi}}} . \quad \text{(A10)}$$

Inspection of Eqn A10 suggests a simple, objective (i.e. independent of measurement precision) criterion to determine the importance of unsteady wake dynamics in locomotive forces: flow unsteadiness should be considered if:

$$\mathrm{Wa} = \frac{c_{ii}}{1 + c_{ii}} . \quad \text{(A11)}$$

Eqn A10 indicates that the left- and right-hand sides of Eqn A11 are equal in the limit of a steady flow ($\mathbf{U_U}=0$), in which case Eqn A5 also holds. Alternatively, where Eqn A11 holds, Eqn A5 is no longer valid, and unsteady wake vortex dynamics must be considered. In general, the wake vortex added-mass tensor will be time-dependent, such that the relative importance of flow unsteadiness varies during the propulsive cycle. For example, in the period during the propulsive cycle when the vortex wake created by *N. bachei* exhibits an added-mass coefficient $c_{ii}=0.6$, the present criterion

suggests that flow unsteadiness contributes to the locomotive force if

$$\frac{\bar{c}_{ii} S U_{Vi}}{\Gamma} = 0.96\,. \qquad \text{(A12)}$$

Whether the unsteady wake vortex dynamics augment the locomotive force or reduce it can only be determined upon further investigation of the fluid dynamics, e.g. using Eqn A6.

List of symbols

$\mathbf{1}$	identity matrix
A	wake vortex shape constant
$\bar{c}_{ii}$	two-dimensional wake vortex added-mass coefficient
c_{ii}	wake vortex added-mass coefficient
$\mathbf{C_{AM}}$	wake vortex added-mass tensor
D	jet diameter
D_V	velar diameter
$\mathbf{e_1}$	unit vector
$\mathbf{F}_L$	locomotive force
ϕ	velocity potential
Γ	vortex circulation
$\mathbf{I}$	total impulse
$\mathbf{I_v}$	vortex impulse
m	body mass
$\mathbf{n}$	normal vector
R	vortex radius
ρ	fluid density
Re	Reynold's number
S	wake vortex width
S_V	vortex surface
t,τ	dimensional time variables
T^*	instantaneous vortex formation time (dimensionless)
T^*_{lim}	vortex formation number (dimensionless)
T^*_{max}	total vortex formation time (dimensionless)
U(t)	jet velocity
$\mathbf{U_{SI}}$	self-induced wake vortex velocity
$\mathbf{U_U}$	unsteady wake vortex velocity
U_{Ui}	unsteady wake vortex speed in *i*-direction
$\mathbf{U_V}$	total wake vortex velocity
U_{Vi}	total wake vortex speed in *i*-direction
V_{OC}	oral cavity volume
V_V	vortex volume
Wa	wake vortex ratio
ω	fluid vorticity
X	body position
$\dot{X}$	body velocity
$\ddot{X}$	body acceleration

This research is supported in part by National Science Foundation Grants OCE-0116236 and OCE-0350834 (to J.H.C.) and OCE-0351398 (to S.P.C.). The authors thank the anonymous reviewers of the manuscript for their thorough and insightful comments.

References

Anderson, E. J. and Grosenbaugh, M. A. (2005). Jet flow in a steadily swimming adult squid. *J. Exp. Biol.* **208**, 1125-1146.

Bartol, I. K., Patterson, M. R. and Mann, R. (2001). Swimming mechanics and behavior of the shallow-water brief squid *Lolliguncula brevis*. *J. Exp. Biol.* **204**, 3655-3682.

Colin, S. P. and Costello, J. H. (2002). Morphology, swimming performance, and propulsive mode of six co-occurring hydromedusae. *J. Exp. Biol.* **205**, 427-437.

Colin, S. P., Costello, J. H. and Klos, E. (2003). In situ swimming and feeding behavior of eight co-occurring hydromedusae. *Mar. Ecol. Prog. Ser.* **253**, 305-309.

Dabiri, J. O. (2005). On the estimation of swimming and flying forces from wake measurements. *J. Exp. Biol.* **208**, 3519-3532.

Dabiri, J. O. (2006). Note on the induced Lagrangian drift and added-mass of a vortex. *J. Fluid Mech.* **547**, 105-113.

Dabiri, J. O. and Gharib, M. (2003). Sensitivity analysis of kinematic approximations in dynamic medusan swimming models. *J. Exp. Biol.* **206**, 3675-3680.

Dabiri, J. O. and Gharib, M. (2004). Fluid entrainment by isolated vortex rings. *J. Fluid Mech.* **511**, 311-331.

Dabiri, J. O. and Gharib, M. (2005a). The role of optimal vortex formation in biological fluid transport. *Proc. R. Soc. Lond. B Biol. Sci.* **272**, 1557-1560.

Dabiri, J. O. and Gharib, M. (2005b). Starting flow through nozzles with temporally variable exit diameter. *J. Fluid Mech.* **538**, 111-136.

Dabiri, J. O., Colin, S. P., Costello, J. H. and Gharib, M. (2005). Flow patterns generated by oblate medusan jellyfish: field measurements and laboratory analyses. *J. Exp. Biol.* **208**, 1257-1265.

Daniel, T. L. (1983). Mechanics and energetics of medusan jet propulsion. *Can. J. Zool.* **61**, 1406-1420.

Daniel, T. L. (1985). Cost of locomotion: unsteady medusan swimming. *J. Exp. Biol.* **119**, 149-164.

Didden, N. (1979). On the formation of vortex rings: rolling-up and production of circulation. *Z. Angew. Math. Phys.* **30**, 101-116.

Donaldson, S., Mackie, G. O. and Roberts, A. (1980). Preliminary observations on escape swimming and giant neurons in *Aglantha digitale* (Hydromedusae: Trachylina). *Can. J. Zool.* **58**, 549-552.

Gharib, M., Rambod, E. and Shariff, K. (1998). A universal time scale for vortex ring formation. *J. Fluid Mech.* **360**, 121-140.

Gladfelter, W. B. (1972). Structure and function of the locomotory system of *Polyorchis montereyensis* (Cnidaria, Hydrozoa). *Helgoländer Wiss. Meeresunters* **23**, 38-79.

Kaplanski, F. B. and Rudi, Y. A. (2005). A model for the formation of 'optimal' vortex rings taking into account viscosity. *Phys. Fluids* **17**, 087101.

Krueger, P. S. and Gharib, M. (2003). The significance of vortex ring formation to the impulse and thrust of a starting jet. *Phys. Fluids* **15**, 1271-1281.

Krueger, P. S., Dabiri, J. O. and Gharib, M. (2003). Vortex ring pinch off in the presence of simultaneously initiated uniform background co-flow. *Phys. Fluids* **15**, L49-L52.

Krueger, P. S., Dabiri, J. O. and Gharib, M. (2006). The formation number of vortex rings formed in uniform background co-flow. *J. Fluid Mech.* **556**, 147-166.

Lamb, H. (1932). *Hydrodynamics*. New York: Dover Publications.

Linden, P. F. and Turner, J. S. (2004). 'Optimal' vortex rings and aquatic propulsion mechanisms. *Proc. R. Soc. Lond. B Biol. Sci.* **271**, 647-653.

Mackie, G. O. (1980). Slow swimming and cyclical fishing behaviour in *Aglantha digitale* (Hydromedusae: Trachylina). *Can. J. Fish. Aquat. Sci.* **37**, 1550-1556.

Milano, M. and Gharib, M. (2005). Uncovering the physics of flapping flat plates with artificial evolution. *J. Fluid Mech.* **534**, 403-409.

Saffman, P. G. (1992). *Vortex Dynamics*. Cambridge: Cambridge University Press.

Smits, A. J. (2000). *A Physical Introduction to Fluid Mechanics*. New York: John Wiley and Sons.